13th ewtec 2019 Proceedings of the 13th European Wave and Tidal Energy Conference 1-6 Sept 2019, Naples, Italy

Sliding Mode Control of an Array of Three Oscillating Water Column Wave Energy Converters to Optimize Electrical Power

Mario E. Magaña, Danielle R. Brown, Daniel T. Gaebele, Joao C. C. Henriques, and Ted K. A. Brekken

Abstract— **This paper presents a complete mathematical model of an array of three oscillating water column (OWC) wave energy converters (WECs) and the design of a direct generator torque control strategy using a sliding mode control (SMC) to maximize the output power of doubly-fed induction generators (DFIGs) attached to bi-radial turbines that are driven by the oscillating motion of the air inside the OWC tubes. The performance of the proposed control strategy is evaluated in irregular waves scenarios and different angles of arrival of the wave front.**

Keywords—**Bi-radial turbine, oscillating water column, sliding mode control, WEC array.**

I. Introduction

OCEAN waves are a promising untapped renewable resource because, in comparison to other renewable resources, ocean waves are dense in power, relatively easy to predict, and have a low variability [1]. These waves are typically found on the western coasts of continents, and engineers are interested in harvesting energy from these waves by deploying large farms of wave energy converters off the coastline, similar to wind turbine farms [2].

Most of the work in the field of wave energy conversion has been done for different types of single wave energy converters (WECs) [3-6], e.g. floating point absorbers (PAs) and oscillating water columns (OWCs). Some research has been done on the dynamic behavior of arrays of uncontrolled WECs arranged in specific configurations and the resulting changes in the wave field and absorbed power have been described. Analyses by various researchers have shown that an array configuration with WECs does not necessarily result in the multiplication of the energy of a single device by the total number of devices [7]. Furthermore, researchers in the field have suggested that wave energy farms could be used to reduce and equalize output fluctuations for a smooth supply of the power grid [8]. Further advantages consist in reduced costs for moorings, grid connections, and maintenance [9].

Our paper presents a hydrodynamic model of three OWCs fully developed from scratch by our research group and its collaborators. Namely, a model that takes into account the frequency dependency of the converters, the hydrodynamic interaction between the three WECs, the effects of the nonlinear dynamical behavior of air inside the chamber of vertical tail tube of the OWC WEC, the dynamics of bi-radial turbine-generators attached to the upper end of the OWC WECs, and the electrical dynamic effects of synchronous DFIGs which transform the mechanical energy delivered by the turbines into electrical energy. In order to design the control algorithm, we cast the 3-OWC WEC array dynamics into a nonlinear state space model of order 21 and then design simple sliding surfaces to force the error between the desired synchronous rotational speed of the DFIG and the rotational speed of the turbine to slide toward zero, in order to achieve rotational speed tracking.

The proposed control strategy is evaluated in irregular waves scenarios and for different angles of arrival of the wave front by means of tests run in the MATLAB/SIMULINK environment. The simulated results provide a validation of the ability of the proposed sliding mode control algorithm to increase the power output of each OWC WEC device.

II. Hydrodynamic Model of WEC Array

Using the model presented in [10] in conjunction with the work from [11], a floating OWC device can be considered as a two-body system, a buoy and an imaginary rigid piston, which represents the internal free surface and allows for the application of oscillating body theory. The piston drives a highly efficient bi-radial

Paper ID number: 1262- Conference track: GPC

M. E. Magaña is with the School of EECS, Oregon State University, 1148 Kelley Engineering Center, Corvallis, OR 97331 USA (e-mail: magana@oregonstate.edu).

D. R. Brown was with the School of EECS, Oregon State University, 1148 Kelley Engineering Center, Corvallis OR 97331 USA (e-mail: danielle.r.brown@uscga.edu).

D. T. Gaebele is with the School of EECS, Oregon State University, 1148 Kelley Engineering Center, Corvallis OR 97331 USA (e-mail: gaebeled@oregonstate.edu).

J. C. C. Henriques is with Technical University of Lisbon, Av. Rovisco Pais, 1049-001, Portugal (e-mail: joaochenriques@tecnico.ulisboa.pt)

T. K. A. Brekken is with the School of EECS, Oregon State University, 1148 Kelley Engineering Center, Corvallis, OR 97331 USA (e-mail: brekken@engr.orst.edu).

turbine, which operates while air is being compressed upwards through the device during a positive heave direction, and back downwards through the turbine during a negative heave direction. In the case of large seas that would damage the turbine, the model closes a stop valve to stop any air flow.

As stated before, we consider three OWC devices in an equilateral triangular array with each buoy moored independently. The mooring configuration is illustrated in Fig. 1, with each device having three mooring cables at an angle β with the sea surface.

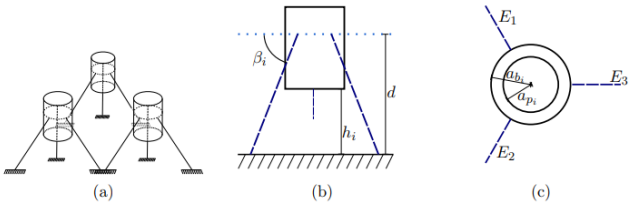

Fig. 1. (a) Triangular WEC array, (b) Side view, (c) Top view.

For this model, small wave amplitudes and body motions are assumed, thus allowing linear water wave theory for the derivation of linear hydrodynamic interactions. The OWC device is assumed to oscillate only in the heave direction, *z*. If each buoy (b) and piston (p) are assumed to only move in the heave direction *z*, then $z = \begin{bmatrix} z_b & z_p \end{bmatrix}^T$.

We simplify the number of forces acting on each buoy and piston to the hydrostatic buoyancy force, the hydrodynamic interaction force, the excitation force, the radiation damping force, the mooring force, and the induced generator force. The generic equation of motion for a single-body system can be stated as

$$m\ddot{z} = F^H + F^G + F^I + F^E + F^R + F^M \tag{1}$$

In [11], a time domain approach was used to derive the dynamic equations for a single WEC and is expanded upon in [12] to a 3 buoy array with three identical WECs. Each buoy and piston will thus be denoted as b_i and p_i. This model also assumes a constant water depth *d* and a clearance to the sea floor h_i.

A. Description of Forces

As stated above, the OWC WEC is restricted to oscillate in the heave (*z*) direction only. An extensive analysis of each of the 6 forces is found in [12], and assuming linear water wave theory, these forces are summarized below.

The hydrostatic buoyancy force is described by:

$$F_{b_i}^H = -\rho_w g S_{b_i} z_{b_i} \tag{2}$$

$$F_{p_i}^H = -\rho_w g S_{p_i} z_{p_i} \tag{3}$$

where ρ_w is the sea water density, *g* is the acceleration of gravity, and *S* is the cross-sectional area.

The control input is the force resulting from the pressure in the air chamber. This is a function of the displaced volume of the OWC and the mass flow rate through the turbine and can be manipulated by the generator torque. The buoy and the piston forces are described by

$$F_{b_i}^G = p_{at} p_i^* S_{p_i} \tag{4}$$

$$F_{p_i}^G = -p_{at} p_i^* S_{p_i} \tag{5}$$

where p_{at} is the atmospheric pressure, and p_i^*, the dimensionless relative pressure, is described by

$$p_i^* = \frac{p_i - p_{at}}{p_{at}} \tag{6}$$

The hydrodynamic interaction force F^I incorporates the added mass due to movements of all the bodies in water. The concept of added mass considers additional forces if an underwater body is accelerating or decelerating or if it is surrounded by an unsteady flow. For the ith buoy in this OWC heaving system, the hydrodynamic interaction force is described by

$$F_{b_i}^I = -\left(\sum_{j=1}^{N} \left(A_{b_i b_j}^{\infty} \ddot{z}_{b_j} + A_{b_i p_j}^{\infty} \ddot{z}_{p_j} \right) \right) \tag{7}$$

$$F_{p_i}^I = -\left(\sum_{j=1}^{N} \left(A_{p_i b_j}^{\infty} \ddot{z}_{b_j} + A_{p_i p_j}^{\infty} \ddot{z}_{p_j} \right) \right) \tag{8}$$

where A_{ij}^{∞} is the added mass of body *i* influenced by the motion of body *j* at infinite frequency, and *N* is equal to 3 for a 3 WEC array.

The local excitation force F^E is the force induced by the waves and is obtained as a superposition of *n* wave-frequency components. This force is described by

$$F_{b_i}^E = \sum_{k=1}^{n} \Gamma_{b_i}(\omega_k, \theta_k) A_k \cos(\omega_k t + \phi_k) \tag{9}$$

$$F_{p_i}^E = \sum_{k=1}^{n} \Gamma_{p_i}(\omega_k, \theta_k) A_k \cos(\omega_k t + \phi_k) \tag{10}$$

where $\Gamma_i(\omega_k, \theta_k)$ is the hydrodynamic excitation coefficients at the radian per second wave frequency ω_k, A_k is the amplitude of the wave, and ϕ_k is the phase of each component which is a random variable governed by a uniform distribution over $[0, 2\pi)$ radians.

The radiation damping force F^R includes the interactions with the motions of other bodies. The forces of body *j* on body *i* can be obtained with the knowledge of the frequency dependent hydrodynamic radiation damping coefficients $B_{ij}(\omega)$. We obtain the impulse

response function (IRF) of the radiation by applying the inverse Fourier transform to $B_{ij}(\omega)$, i.e.

$$K_{ij}(t) = \frac{2}{\pi}\int_0^\infty B_{ij}(\omega)cos(\omega t)d\omega. \quad (11)$$

The convolution integral over the IRF and the body motion leads to the radiation force F^R, taking into account all the past and present events.

$$F_{ij}^R = -\int_0^t K_{ij}(t-\tau)\dot{z}_j(\tau)d\tau \quad (12)$$

All distinct IRFs converge to zero if the time is large enough, wherefore the kernel $K(t)$ can be approximated with a sum of complex exponentials, as applied in [16], i.e.

$$K_{ij}(t) = \sum_{k=1}^{N_{ij}} \alpha_{ij,k} e^{\beta_{ij,k}t}, \quad (13)$$

where N_{ij} is the number of exponential functions and this order of approximation varies for different body combinations *i*, *j*, and α_k and β_k are the complex Prony coefficients, which will be determined with the Prony method. Substituting (13) into the convolution integral (12), yields

$$\begin{aligned} F_{ij}^R &= -\int_0^t \sum_{k=1}^{N_{ij}} \alpha_{ij,k} e^{\beta_{ij,k}(t-\tau)}\dot{z}_j(\tau)d\tau \\ &= -\sum_{k=1}^{N_{ij}} \alpha_{ij,k} e^{\beta_{ij,k}t}\int_0^t e^{\beta_{ij,k}(-\tau)}\dot{z}_j(\tau)d\tau \end{aligned}. \quad (14)$$

Taking the derivative of (14) with respect to time gives

$$\dot{F}_{ij}^R = -\sum_{k=1}^{N_{ij}}\left(\beta_{ij,k}\underbrace{\alpha_{ij,k}e^{\beta_{ij,k}t}\dot{z}_j(\tau)d\tau}_{F_{ij,k}^R} + \alpha_{ij,k}e^{\beta_{ij,k}t}e^{-\beta_{ij,k}t}\dot{z}_j(t)\right) \quad (15)$$

$$\dot{F}_{ij}^R = -\sum_{k=1}^{N_{ij}}\left(\beta_{ij,k}F_{ij,k}^R + \alpha_{ij,k}\dot{z}_j\right), \quad (16)$$

where the different $F_{ij}^R, k \in \{1\cdots N_{ij}\}$ will be introduced as a separate state vector $f_{ij}^R = \left[F_{ij,1}^R \cdots F_{ij,N_{ij}}^R\right]^T$ to write the change rate of the radiation force in a linear state space representation, namely,

$$\dot{f}_{ij}^R = \underbrace{\mathrm{diag}(\beta_{ij,1}\cdots\beta_{ij,N_{ij}})}_{A_{ij}^R}\cdot f_{ij}^R + \underbrace{\left[\alpha_{ij,1}\cdots\alpha_{ij,N_{ij}}\right]^T}_{(b_{ij}^R)^T}\cdot\dot{z}_j \quad (17)$$

$$F_{ij}^R = \underbrace{\mathrm{ones}\left(N_{ij}\right)}_{c_{ij}^R}\cdot f_{ij}^R. \quad (18)$$

The term diag(·) denotes a square diagonal matrix with the arguments as elements on its main diagonal, yielding the dynamic matrix A_{ij}^R. The term ones(·) denotes a vector with ones of length of the argument resulting in the output vector c_{ij}^R. The input vector b_{ij}^R consists of the Prony amplitude coefficients $\alpha_{ij,k}$. This state space representation has the velocity of the influencing body $\dot{z}_j$ as input, the single decaying exponential approximations as elements of f_{ij} as states and the superposition of those vector entries as output F_{ij}^R. The order of the state space depends on the order of the applied Prony method to achieve the best fit to the IRF. To calculate the radiation force on a body *i* we need to take all the bodies $j \in \{b_1, b_2, b_3, p_1, p_2, p_3\}$ into account, i.e.

$$F_i^R = \sum_j F_{ij}^R = \sum_j c_{ij}^R \cdot f_{ij}^R. \quad (19)$$

In the notation of the buoy and piston for the array of *N* = 3 devices this force can be stated as a sum of the individual forces between each body and is defined as,

$$F_{b_i}^R = \sum_{j=1}^{N}\left(F_{b_ib_j}^R + F_{b_ip_j}^R\right) = \sum_{j=1}^{N_b}\left(c_{b_ib_j}^R f_{b_ib_j}^R + c_{b_ip_j}^R f_{b_ip_j}^R\right) \quad (20)$$

$$F_{p_i}^R = \sum_{j=1}^{N}\left(F_{p_ib_j}^R + F_{p_ip_j}^R\right) = \sum_{j=1}^{N_b}\left(c_{p_ib_j}^R f_{p_ib_j}^R + c_{p_ip_j}^R f_{p_ip_j}^R\right) \quad (21)$$

where ***c*** is a vector of ones of length N_{ij} and *f* is a single decaying exponential approximation.

For the mooring force F^M, it is assumed that the whole system movement is linear and variations in the mean surface value are ignored. All mooring lines are attached at the intersection from the free surface with the buoy at the angle β which is assumed to be constant, due to the higher length of the cables compared to the body movement. The mooring forces are described by

$$F_{b_i}^M = -3K\sin^2(\beta)z_{bi} \quad (22)$$

$$F_{p_i}^M = 0 \quad (23)$$

where *K* is the spring coefficient of the cable, and β is the angle the mooring line is attached to the free surface.

B. Biradial Turbine

In the work of [11], the air turbine chosen for the OWC WEC is a biradial turbine. The dynamics of the air in the chamber of this turbine are described by

$$\dot{p}^* = -\frac{\gamma}{V_c}(p^*+1)\dot{V}_c - \frac{\gamma}{\rho_{at}V_c}(p^*+1)^{\frac{\gamma-1}{\gamma}}\dot{m}_t \quad (24)$$

where $V_c(z_b, z_p)$ is the air volume in cylindrical chamber of WEC, ρ_{at} is the atmospheric air density. Furthermore, $\dot{m}_t = (1-P_{hssv})\rho_{in}d_t^3\Phi\Omega$ is the turbine mass flow rate, $\rho_{in} = \rho_{at}max(p^*+1,1)^{1/\gamma}$ is the reference air density,

$\gamma = \frac{c_p}{c_v} \cong 1.4$ is the specific heat ratio of air,

$\Phi = \frac{\dot{m}_t}{\rho_{in}\Omega d_t^3}$ is the dimensionless air flow coefficient,

$\Psi = \frac{p_{at}p^*}{\rho_{in}\Omega^2 d_t^2}$ is the dimensionless pressure head,

$\eta_t = \frac{P_t}{\rho_{in} d_t^5 \Phi\Psi}$ is the turbine efficiency,

d_t diameter of turbine rotor, P_t power delivered by turbine and P_{hssv} is the position of the stop valve, open for $P_{hssv} = 0$ and closed for $P_{hssv} = 1$.

The power of the turbine is defined as

$$P_t = T_t\Omega = \rho_{in}\eta_t d_t^5 \Phi\Psi\Omega^3 \tag{25}$$

where Ω is the speed of the turbine. Therefore,

$$T_t = \rho_{in}\eta_t d_t^5 \Phi\Psi\Omega^2. \tag{26}$$

The generator-turbine dynamical equation for this model can be described by

$$J\dot{\Omega} + B\Omega = T_t - T_g, \tag{27}$$

where *J* is the generator-turbine rotor moment of inertia, B is the coefficient of viscous friction, T_t is the turbine torque, and T_g is the generator torque.

Substituting (26) into (27), the rotational dynamics become,

$$J\dot{\Omega} + B\Omega = \rho_{in}\eta_t d_t^5 \Phi\Psi\Omega^2 - T_g \tag{28}$$

C. State Space Model

The state space model was developed in the work of [12]. Substituting equations (2), (3), (4), (5), (7), (8), (9), (10), (20), (21), (22), and (23), into equation (1), and using equations (24) and (28) leads to the equations of motion of the system $i, i = 1, 2, 3$

$$m_{b_i}\ddot{z}_{b_i} = -\rho_w g S_{b_i} z_{b_i} + p_{at} S_{p_i} p_i^* + F_{b_i}^E + F_{b_i}^M + F_{b_i}^I + F_{b_i}^R \tag{29}$$

$$m_{p_i}\ddot{z}_{p_i} = -\rho_w g S_{p_i} z_{p_i} + p_{at} S_{p_i} p_i^* + F_{p_i}^E + F_{p_i}^I + F_{p_i}^R \tag{30}$$

$$\dot{p}_i^* = \frac{-\gamma}{h_0 + z_{b_i} - z_{p_i}}\left(\frac{\dot{m}_{t,i}}{\rho_{at} S_{p_i}}(p^* + 1)^{\frac{\gamma-1}{\gamma}} + (p^* + 1)(\dot{z}_{b_i} - \dot{z}_{p_i})\right) \tag{31}$$

Let us introduce the state vector $x \in \mathbb{R}^{18x1}$. This vector will consist of the vertical positions x_{pos} and velocities x_{vel} of all buoys and pistons, the dimensionless pressures x_{pres} and the rotational kinetic energies x_{kin}. This state vector can be described as

$$x = \begin{bmatrix} x_{pos} & x_{vel} & x_{pres} & x_{kin} \end{bmatrix}^T \tag{32}$$

$$x_{pos} = \begin{bmatrix} z_{b_1} \\ z_{b_2} \\ z_{b_3} \\ z_{p_1} \\ z_{p_2} \\ z_{p_3} \end{bmatrix}, x_{vel} = \begin{bmatrix} \dot{z}_{b_1} \\ \dot{z}_{b_2} \\ \dot{z}_{b_3} \\ \dot{z}_{p_1} \\ \dot{z}_{p_2} \\ \dot{z}_{p_3} \end{bmatrix}, x_{pres} = \begin{bmatrix} p_1^* \\ p_2^* \\ p_3^* \end{bmatrix}, x_{kin} = \begin{bmatrix} \Omega_1 \\ \Omega_2 \\ \Omega_3 \end{bmatrix} \tag{33}$$

If we let the control input be described as

$$\boldsymbol{u} = \begin{bmatrix} T_{g,1} & T_{g,2} & T_{g,3} & P_{hssv,1} & P_{hssv,2} & P_{hssv,3} \end{bmatrix} \tag{34}$$

the equations of motion can now be expressed in a state space representation as

$$\dot{\boldsymbol{x}} = \begin{bmatrix} \dot{x}_1 \\ \dot{x}_2 \\ \dot{x}_3 \\ \dot{x}_4 \\ \dot{x}_5 \\ \dot{x}_6 \\ \dot{x}_7 \\ \dot{x}_8 \\ \dot{x}_9 \\ \dot{x}_{10} \\ \dot{x}_{11} \\ \dot{x}_{12} \\ \dot{x}_{13} \\ \dot{x}_{14} \\ \dot{x}_{15} \\ \dot{x}_{16} \\ \dot{x}_{17} \\ \dot{x}_{18} \end{bmatrix} = \begin{bmatrix} \dot{z}_{b_1} \\ \dot{z}_{b_2} \\ \dot{z}_{b_3} \\ \dot{z}_{p_1} \\ \dot{z}_{p_2} \\ \dot{z}_{p_3} \\ \ddot{z}_{b_1} \\ \ddot{z}_{b_2} \\ \ddot{z}_{b_3} \\ \ddot{z}_{p_1} \\ \ddot{z}_{p_2} \\ \ddot{z}_{p_3} \\ \dot{p}_1^* \\ \dot{p}_2^* \\ \dot{p}_3^* \\ \dot{\Omega}_1 \\ \dot{\Omega}_2 \\ \dot{\Omega}_3 \end{bmatrix} = \begin{bmatrix} x_7 \\ x_8 \\ x_9 \\ x_{10} \\ x_{11} \\ x_{12} \\ \dot{x}_{vel}(1) \\ \dot{x}_{vel}(2) \\ \dot{x}_{vel}(3) \\ \dot{x}_{vel}(4) \\ \dot{x}_{vel}(5) \\ \dot{x}_{vel}(6) \\ f_{p,1} \\ f_{p,2} \\ f_{p,3} \\ f_{t,1} \\ f_{t,2} \\ f_{t,3} \end{bmatrix} \tag{35}$$

where $\begin{bmatrix} f_{p,1} & f_{p,2} & f_{p,3} \end{bmatrix}^T$ is equal to

$$\begin{bmatrix} \frac{-\gamma}{(h_0 + x_1 - x_4)}\left(\frac{\dot{m}_{t,1}}{\rho_{at} S_{p_i}}(x_{13} + 1)^{\frac{\gamma-1}{\gamma}} + (x_{13} + 1)(x_7 - x_{10})\right) \\ \frac{-\gamma}{(h_0 + x_2 - x_5)}\left(\frac{\dot{m}_{t,2}}{\rho_{at} S_{p_i}}(x_{14} + 1)^{\frac{\gamma-1}{\gamma}} + (x_{14} + 1)(x_8 - x_{11})\right) \\ \frac{-\gamma}{(h_0 + x_3 - x_6)}\left(\frac{\dot{m}_{t,3}}{\rho_{at} S_{p_i}}(x_{15} + 1)^{\frac{\gamma-1}{\gamma}} + (x_{15} + 1)(x_9 - x_{12})\right) \end{bmatrix} \tag{36}$$

where $\dot{m}_{t,i} = f(x_{i+15}, u_{i+3})$ and

$$\begin{bmatrix} f_{t,1} \\ f_{t,2} \\ f_{t,3} \end{bmatrix} = \begin{bmatrix} \frac{1}{J}(\rho_{in_1}(x_{16})^2 d_t^5 \eta_{t_i} \Phi_i \Psi_i - u_1) \\ \frac{1}{J}(\rho_{in_2}(x_{17})^2 d_t^5 \eta_{t_i} \Phi_i \Psi_i - u_2) \\ \frac{1}{J}(\rho_{in_3}(x_{18})^2 d_t^5 \eta_{t_i} \Phi_i \Psi_i - u_3) \end{bmatrix} \tag{37}$$

together with

$\Psi_i = f(x_{i+12}), \Phi_i = f(\Psi_i), \eta_{t_i} = f(\Psi_i), i \in \{1,2,3\})$ and finally

$$\dot{x}_{vel} = \underbrace{\begin{bmatrix} M_{b_1} & A^{\infty}_{b_1 b_2} & A^{\infty}_{b_1 b_3} & A^{\infty}_{b_1 p_1} & A^{\infty}_{b_1 p_2} & A^{\infty}_{b_1 p_3} \\ A^{\infty}_{b_2 b_1} & M_{b_2} & A^{\infty}_{b_2 b_3} & A^{\infty}_{b_2 p_1} & A^{\infty}_{b_2 p_2} & A^{\infty}_{b_2 p_3} \\ A^{\infty}_{b_3 b_1} & A^{\infty}_{b_3 b_2} & M_{b_3} & A^{\infty}_{b_2 p_1} & A^{\infty}_{b_3 p_2} & A^{\infty}_{b_3 p_3} \\ A^{\infty}_{p_1 b_1} & A^{\infty}_{p_3 b_2} & A^{\infty}_{p_1 b_3} & M_{p_1} & A^{\infty}_{p_1 p_2} & A^{\infty}_{p_1 p_3} \\ A^{\infty}_{p_2 b_1} & A^{\infty}_{p_2 b_2} & A^{\infty}_{p_2 b_3} & A^{\infty}_{p_2 p_1} & M_{p_2} & A^{\infty}_{p_2 p_3} \\ A^{\infty}_{p_3 b_1} & A^{\infty}_{p_3 b_2} & A^{\infty}_{p_3 b_3} & A^{\infty}_{p_3 p_1} & A^{\infty}_{p_3 p_2} & M_{p_3} \end{bmatrix}^{-1}}_{\mathbf{A}_{\infty}^{-1}} \underbrace{\begin{bmatrix} F_{b1} \\ F_{b2} \\ F_{b3} \\ F_{p1} \\ F_{p2} \\ F_{p3} \end{bmatrix}}_{\underline{F}} \tag{38}$$

with $M_n = m_n + A^{\infty}_{nn}, n \in \{b_1, b_2, b_3, p_1, p_2, p_3\}$,

$$\underline{F} = \underbrace{diag(x_{pos}) \cdot \begin{bmatrix} -\rho_w g S_{b1} \\ -\rho_w g S_{b2} \\ -\rho_w g S_{b3} \\ -\rho_w g S_{p1} \\ -\rho_w g S_{p2} \\ -\rho_w g S_{p3} \end{bmatrix}}_{\mathbf{F}^B} + \underbrace{diag(x_{pres}, x_{pres}) \cdot \begin{bmatrix} p_{at} S_{p1} \\ p_{at} S_{p2} \\ p_{at} S_{p3} \\ -p_{at} S_{p1} \\ -p_{at} S_{p2} \\ -p_{at} S_{p3} \end{bmatrix}}_{\mathbf{F}^G}$$

$$- \underbrace{\begin{bmatrix} 3Ksin^2(\beta) z_{b1} \\ 3Ksin^2(\beta) z_{b2} \\ 3Ksin^2(\beta) z_{b3} \\ 0 \\ 0 \\ 0 \end{bmatrix}}_{\mathbf{F}^M} + \mathbf{C}^R \circ \mathbf{F}^R \underbrace{\begin{bmatrix} 1 \\ 1 \\ 1 \\ 1 \\ 1 \\ 1 \end{bmatrix}}_{\mathbf{F}^R} + \underbrace{\begin{bmatrix} \sum_{k=1}^{n} \Gamma_{b1}(\omega_k) A_k cos(\omega_k t + \phi_k) \\ \sum_{k=1}^{n} \Gamma_{b2}(\omega_k) A_k cos(\omega_k t + \phi_k) \\ \sum_{k=1}^{n} \Gamma_{b3}(\omega_k) A_k cos(\omega_k t + \phi_k) \\ \sum_{k=1}^{n} \Gamma_{p1}(\omega_k) A_k cos(\omega_k t + \phi_k) \\ \sum_{k=1}^{n} \Gamma_{p2}(\omega_k) A_k cos(\omega_k t + \phi_k) \\ \sum_{k=1}^{n} \Gamma_{p3}(\omega_k) A_k cos(\omega_k t + \phi_k) \end{bmatrix}}_{\mathbf{F}^E} \tag{39}$$

and

$$\underline{C}^R = \begin{bmatrix} c^R_{b_1 b_1} & c^R_{b_1 b_2} & c^R_{b_1 b_3} & c^R_{b_1 p_1} & c^R_{b_1 p_2} & c^R_{b_1 p_3} \\ c^R_{b_2 b_1} & c^R_{b_2 b_2} & c^R_{b_2 b_3} & c^R_{b_2 p_1} & c^R_{b_2 p_2} & c^R_{b_2 p_3} \\ c^R_{b_3 b_1} & c^R_{b_3 b_2} & c^R_{b_3 b_3} & c^R_{b_2 p_1} & c^R_{b_3 p_2} & c^R_{b_3 p_3} \\ c^R_{p_1 b_1} & c^R_{p_3 b_2} & c^R_{p_1 b_3} & c^R_{p_1 b_1} & c^R_{p_1 p_2} & c^R_{p_1 p_3} \\ c^R_{p_2 b_1} & c^R_{p_2 b_2} & c^R_{p_2 b_3} & c^R_{p_2 p_1} & c^R_{p_2 p_2} & c^R_{p_2 p_3} \\ c^R_{p_3 b_1} & c^R_{p_3 b_2} & c^R_{p_3 b_3} & c^R_{p_3 p_1} & c^R_{p_3 p_2} & c^R_{p_3 p_3} \end{bmatrix} \tag{40}$$

$$\underline{F}^R = \begin{bmatrix} f^R_{b_1 b_1} & f^R_{b_1 b_2} & f^R_{b_1 b_3} & f^R_{b_1 p_1} & f^R_{b_1 p_2} & f^R_{b_1 p_3} \\ f^R_{b_2 b_1} & f^R_{b_2 b_2} & f^R_{b_2 b_3} & f^R_{b_2 p_1} & f^R_{b_2 p_2} & f^R_{b_2 p_3} \\ f^R_{b_3 b_1} & f^R_{b_3 b_2} & f^R_{b_3 b_3} & f^R_{b_2 p_1} & f^R_{b_3 p_2} & f^R_{b_3 p_3} \\ f^R_{p_1 b_1} & f^R_{p_3 b_2} & f^R_{p_1 b_3} & f^R_{p_1 b_1} & f^R_{p_1 p_2} & f^R_{p_1 p_3} \\ f^R_{p_2 b_1} & f^R_{p_2 b_2} & f^R_{p_2 b_3} & f^R_{p_2 p_1} & f^R_{p_2 p_2} & f^R_{p_2 p_3} \\ f^R_{p_3 b_1} & f^R_{p_3 b_2} & f^R_{p_3 b_3} & f^R_{p_3 p_1} & f^R_{p_3 p_2} & f^R_{p_3 p_3} \end{bmatrix}. \tag{41}$$

The Schur product of the matrices responsible for the radiation force F^R are denoted by $\circ$. As previously discussed, every entry of $\underline{F}^R$ is a state vector itself. The dynamics of the entries follow (17) and denote the time derivative of every entry. This yields the matrix form of the dynamics of this subsystem, namely,

$$\dot{\underline{F}}^R = \underline{A}^R \circ \underline{F}^R + \underline{B}^R \circ \begin{bmatrix} x^T_{vel} \\ x^T_{vel} \\ x^T_{vel} \\ x^T_{vel} \\ x^T_{vel} \\ x^T_{vel} \end{bmatrix}, \tag{42}$$

where

$$\underline{A}^R = \begin{bmatrix} A^R_{b_1 b_1} & A^R_{b_1 b_2} & A^R_{b_1 b_3} & A^R_{b_1 p_1} & A^R_{b_1 p_2} & A^R_{b_1 p_3} \\ A^R_{b_2 b_1} & A^R_{b_2 b_2} & A^R_{b_2 b_3} & A^R_{b_2 p_1} & A^R_{b_2 p_2} & A^R_{b_2 p_3} \\ A^R_{b_3 b_1} & A^R_{b_3 b_2} & A^R_{b_3 b_3} & A^R_{b_2 p_1} & A^R_{b_3 p_2} & A^R_{b_3 p_3} \\ A^R_{p_1 b_1} & A^R_{p_3 b_2} & A^R_{p_1 b_3} & A^R_{p_1 b_1} & A^R_{p_1 p_2} & A^R_{p_1 p_3} \\ A^R_{p_2 b_1} & A^R_{p_2 b_2} & A^R_{p_2 b_3} & A^R_{p_2 p_1} & A^R_{p_2 p_2} & A^R_{p_2 p_3} \\ A^R_{p_3 b_1} & A^R_{p_3 b_2} & A^R_{p_3 b_3} & A^R_{p_3 p_1} & A^R_{p_3 p_2} & A^R_{p_3 p_3} \end{bmatrix}, \tag{43}$$

and

$$\underline{B}^R = \begin{bmatrix} b^R_{b_1b_1} & b^R_{b_1b_2} & b^R_{b_1b_3} & b^R_{b_1p_1} & b^R_{b_1p_2} & b^R_{b_1p_3} \\ b^R_{b_2b_1} & b^R_{b_2b_2} & b^R_{b_2b_3} & b^R_{b_2p_1} & b^R_{b_2p_2} & b^R_{b_2p_3} \\ b^R_{b_3b_1} & b^R_{b_3b_2} & b^R_{b_3b_3} & b^R_{b_3p_1} & b^R_{b_3p_2} & b^R_{b_3p_3} \\ b^R_{p_1b_1} & b^R_{p_1b_2} & b^R_{p_1b_3} & b^R_{p_1b_1} & b^R_{p_1p_2} & b^R_{p_1p_3} \\ b^R_{p_2b_1} & b^R_{p_2b_2} & b^R_{p_2b_3} & b^R_{p_2p_1} & b^R_{p_2p_2} & b^R_{p_2p_3} \\ b^R_{p_3b_1} & b^R_{p_3b_2} & b^R_{p_3b_3} & b^R_{p_3p_1} & b^R_{p_3p_2} & b^R_{p_3p_3} \end{bmatrix}. \quad (44)$$

III. GENERATOR MODEL

To convert the mechanical power into electrical power, we need to attach a generator to the air turbine. In this work we use a doubly fed induction generator DFIG, which is described by the following equations [13]:

$$i_{qs} = -\frac{L_m}{L_s} i_{qr} \quad (45)$$

$$i_{ds} = \frac{L_m}{L_s}\left(i_{ms} - i_{dr}\right) \quad (46)$$

$$i_{ms} = \frac{v_{qs} - r_s i_{qs}}{\Omega_s L_m} \quad (47)$$

$$T_g = -\frac{3p}{4}\left(\frac{L_m^2 i_{ms} i_{qr}}{L_s}\right) = -k_g i_{qr} \quad (48)$$

$$k_g = \frac{3p}{4}\left(\frac{L_m^2 i_{ms}}{L_s}\right) \quad (49)$$

$$Q_s = \frac{3\Omega_s L_m^2 i_{ms}\left(i_{ms} - i_{dr}\right)}{2L_s} \quad (50)$$

$$v_{dr} = r_r i_{dr} + \sigma\left(L_r \frac{di_{qr}}{dt} - \Delta\Omega_s L_r i_{qr}\right) \quad (51)$$

$$v_{qr} = r_r i_{qr} + \sigma L_r \frac{di_{qr}}{dt} + \Delta\Omega_s\left(\sigma L_r i_{dr} + \frac{L_m^2 i_{ms}}{L_s}\right) \quad (52)$$

$$\Delta\Omega_s = \Omega_s - \Omega \quad (53)$$

$$\sigma = 1 - \frac{L_m^2}{L_s L_r} \quad (54)$$

where L_s is the stator inductance, L_r is the rotor inductance, L_m is the mutual inductance, Ω_s is the synchronous speed, Ω is the generator rotor speed, r_r is the rotor resistance, i_{ms} is the stator magnetizing current, p is the number of poles, r_s is the stator resistance, i_{qs} is the q-axis stator current, i_{qr} is the q-axis rotor current, i_{ds} is the d-axis stator current, i_{dr} is the d-axis rotor current, v_{qs} is the q-axis stator voltage, v_{dr} is the d-axis rotor voltage, and v_{qr} is the q-axis rotor voltage.

IV. CONTROLLER DESIGN

Control of the generator electromagnetic torque, T_g, implies q-axis rotor current control (see (50)). Substituting (50) into (28), yields

$$\frac{d\Omega}{dt} = -\frac{B}{J}\Omega + \frac{\rho_{in}\eta_t d^5 \Phi\Psi}{J}\Omega^2 + \frac{k_g}{J} i_{qr} \quad (55)$$

The turbine torque is defined by

$$T_t \equiv \rho_{in}\eta_t d^5 \Phi\Psi\Omega^2 . \quad (56)$$

Let $a = \frac{B}{J}$, $b = \frac{k_g}{J}$, and $i_{eq} = \frac{T_t}{k_g}$, then (55) becomes

$$\dot{\Omega} = -a\Omega + bi_{eq} + bi_{qr} . \quad (57)$$

Our goal here is to control the q-axis rotor current i_{qr} in such a way as to force the turbine speed to track the synchronous speed of the DFIG.

D. Sliding Mode Control (SMC)

SMC is a robust control method that can handle sudden and large changes to system dynamics. It has many applications including DC/DC and AC/DC power converters, AC and DC motors and generators, aircraft and missile guidance and control, and robotic control. SMC essentially uses discontinuous feedback control laws to force the system state to reach and remain on a specified surface. It requires the proper design of a sliding variable, $\sigma(t)$, and once $\sigma(t) = 0$, it defines the sliding surface.

There is a two-step procedure for SMC design. The first step includes designing a switching function so that the system motion on the sliding surface satisfies the design requirements. The second step includes the selection of a control law which forces the system trajectory to the sliding surface and remains there [18].

To design our SMC law, we begin by defining an error signal equal to the difference between the actual rotational speed of the turbine/generator $\Omega(t)$ and the desired rotational speed of the turbine/generator $\Omega_d(t)$, that is to say, $e(t) = \Omega(t) - \Omega_d(t)$. Then the acceleration error is given by

$$\begin{aligned} \dot{e}(t) &= \dot{\Omega}(t) - \dot{\Omega}_d(t) \\ &= -ae(t) - a\Omega_d(t) + b\left[i_{eq}(t) + i_{qr}(t)\right] - \dot{\Omega}_d(t) \end{aligned} \quad (58)$$

Our goal is to drive the error dynamics to zero at least asymptotically in a short period of time. To do so, we select a simple sliding surface described by

$$\sigma(t) = se(t), \tag{59}$$

where s is a design parameter. Once on the sliding surface, $\sigma(t) = 0$ and

$$\begin{aligned}\dot{\sigma}(t) &= s\dot{e}(t)\\ &= -s\left[ae(t) + a\Omega_d(t) - b\left[i_{eq}(t) + i_{qr}(t)\right] + \dot{\Omega}_d(t)\right]\\ &= 0\end{aligned} \tag{60}$$

Let $T_g = T_t$, then

$$i_{eq}(t) = \frac{\rho_{in}\eta_t d^5 \Phi\Psi}{k_g}\Omega^2(t) \tag{61}$$

and

$$\left|i_{eq}(t)\right| \le \max\left\{\frac{\rho_{in}\eta_t d^5 \Phi\Psi}{k_g}\Omega^2(t)\right\}. \tag{62}$$

From [11],

$$\Psi = k_\Psi \Phi^{5/3} \tag{63}$$

Define the function $\xi(t,e)$ as

$$\begin{aligned}\xi(t,e) &\equiv \max\left\{\frac{\rho_{in}\eta_t d^5 \Phi\Psi}{k_g}\Omega^2(t)\right\}\\ &= d^5 \max\left\{\frac{k_\Psi \rho_{in}\eta_t \Phi^{8/3}\Omega^2}{k_g}\right\}\end{aligned} \tag{64}$$

Assuming we can control the q-axis rotor current and we only know the bounds of $i_{eq}(t)$, let

$$\zeta(t,e) \equiv \left(\beta + \xi(t,e)\left|sb\right|\right)\mathrm{sgn}\left(\sigma(t)\right),\ \beta > 0 \tag{65}$$

and

$$sbi_{qr}(t) = sae(t) + sa\Omega_d(t) + s\dot{\Omega}_d(t) - \zeta(t,e) \tag{66}$$

or

$$i_{qr}(t) = \frac{a}{b}e(t) + \frac{a}{b}\Omega_d(t) + \frac{1}{b}\dot{\Omega}_d(t) - \frac{1}{sb}\zeta(t,e) \tag{67}$$

where $\xi(t,e)$ is such that $\left|i_{eq}(t)\right| \le \xi(t,e)$.

E. Stability of Sliding Mode Controlled System

Let the Lyapunov function be given by

$$V(t) = 0.5\sigma(t)^2. \tag{68}$$

Then

$$\dot{V}(t) = \sigma(t)\dot{\sigma}(t) \tag{69}$$

and

$$\begin{aligned}\dot{\sigma}(t) &= sbi_{eq}(t) - \beta\,\mathrm{sgn}(\sigma(t)) - \xi(t,e)\left|sb\right|\mathrm{sgn}(\sigma(t))\\ &= sbi_{eq}(t) - \zeta(t,e)\end{aligned}. \tag{70}$$

But,

$$sbi_{eq}(t) \le \left|sb\right|\left|i_{eq}(t)\right| \le \left|sb\right|\xi(t,e). \tag{71}$$

Thus,

$$\begin{aligned}\sigma(t)\dot{\sigma}(t) &= \sigma(t)\left[sbi_{eq}(t) - \zeta(t,e)\right]\\ &\le |\,sb\,||\,\sigma(t)\,|\,\xi(t,e) - \sigma(t)\zeta(t,e)\end{aligned}. \tag{72}$$

Now,

$$\begin{aligned}\sigma(t)\zeta(t,e) &= \beta\sigma(t)\,\mathrm{sgn}\left(\sigma(t)\right) + |\,sb\,|\,\sigma(t)\,\mathrm{sgn}\left(\sigma(t)\right)\xi(t,e)\\ &= \beta\,|\,\sigma(t)\,| + |\,sb\,||\,\sigma(t)\,|\,\xi(t,e)\end{aligned}$$

Hence,

$$\dot{V}(t) = \sigma(t)\dot{\sigma}(t) \le -\beta\,|\,\sigma(t)\,| < 0, \forall\sigma(t) \ne 0, \tag{73}$$

which says that the error system is asymptotically stable and thus the generator angular velocity follows the desired angular velocity at least asymptotically.

V. PERFORMANCE EVALUATION

The control law $i_{qr}(t)$ is implemented for an array of 3 Marmok buoy's that have a separation of 40 m using MATLAB/SIMULINK. The parameters of this model are found in the appendix. The simulation starts from a rest position, namely all the initial conditions are equal to zero, except for the rotational speed of the turbine which is set to 950 rpm, as the turbines cannot start from rest. The experiment starts at t = 50 s which is when the system reaches a steady state, and ends after 5 minutes have passed. Only the results of buoy 1 in the WEC system is presented to discuss the results without overcrowding the graphs with too much information. The WEC system is subjected to incident waves which are irregular in nature.

In the work of [11] and [12], a physical generator was not attached to the bi-radial turbine of the OWC WEC model. However, an optimal theoretical torque control (here called ideal) that maximizes mechanical power was developed and is described by

$$T_g = -0.0001\Omega^{2.6}, \tag{74}$$

We shall refer to this control as the ideal control law.

Figure 2 depicts the 3 buoy array configuration with a range of wave incidence angles, θ, between -60 degrees and +60 degrees. During the design of the SMC controller, θ was set to 60 degrees.

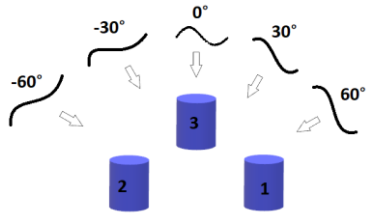

Fig. 2. Range of wave incidence angle.

F. Buoy Motion and System Forces

The motion of buoy 1 can be seen in Fig. 3. When the buoy is around its local minimum in its oscillation and the wave is rising, a high excitation occurs and the buoy's movement is amplified, as seen around t = 170 s. On the other hand, if the buoy is around its local maximum and the wave is falling, a destructive interference happens, which is seen around t = 210 s. The forces involved in the simulation are depicted in Fig. 4. The restoring force is the largest force and the control force is the one induced by the generator.

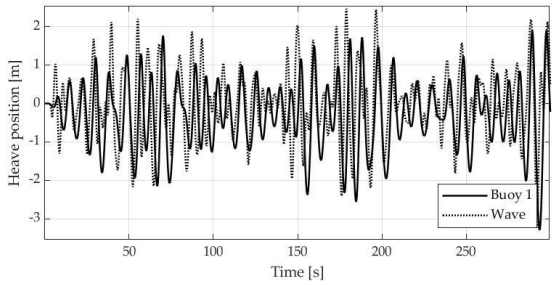

Fig. 3. Buoy 1 motion in irregular waves.

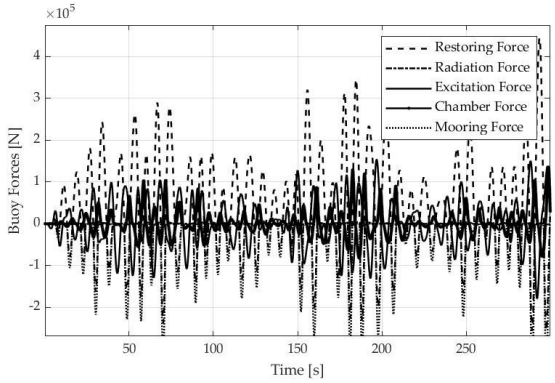

Fig. 4. Forces on buoy 1.

G. Ideal Control Law Performance

We first apply the ideal control law (74). Fig. 5 shows the rotational speed of the turbine for buoy 1, where we can see the speed ranges in value from 750 to 2250 rpm. The average rotational speed is 1316 rpm. Fig. 6 shows the generated power for buoy 1. The average power generated using (74) for buoy 1 was 2.46 kW. One of the methods to evaluate performance is to determine the efficiency of the generator in converting the available turbine mechanical power into electrical power. The average efficiency of the generator for the ideal control law is 84.65%.

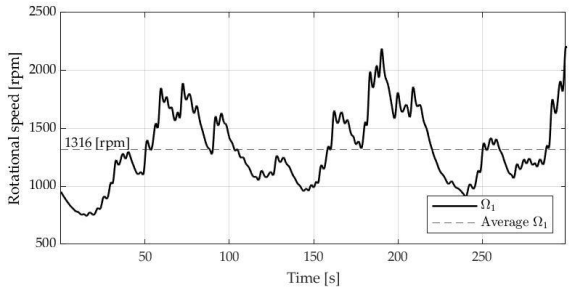

Fig. 5. Buoy 1 rotational speed using ideal control law.

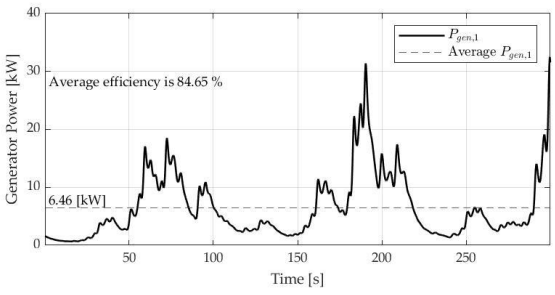

Fig. 6. Buoy 1 generated power using ideal control law.

H. Proposed Sliding Mode Control Performance

Following the work of [20], the parameters for the DFIG are listed on table 1

TABLE 1
DFIG PARAMETERS

$p = 2$	$L_m = 7.413$ H
$R_s = 0.0181\ \Omega$	$L_s = 0.13$ H
$R_r = 0.0334\ \Omega$	$L_r = 0.16$ H
$B = 0.01$ N-m-s	$J = 3.06$ kg-m^2

Although the SMC controller developed in this paper is different that the SMC controller developed in the work of [16], the parameters were first chosen based off the work of [16] to achieve initial results. It is important to also note that $\dot{u}_r = 0$. Thus, the SMC controller parameter β was set to 30 and the parameter s was set to 0.1. Also using the work of [17] as a guide, the parameter of i_{ms} was set to 170 mH. Using the average rotational speed of the uncontrolled system as a starting point, the desired rotational speed Ω_d was set to 1200 rpm.

While in the sliding mode, the state variables will exhibit oscillations around the switching surface. In an ideal system, these oscillations would approach infinity and the system would slide perfectly along the sliding surface. However, due to imperfections such as delay, these oscillations are of a finite nature and produce chattering, where the system zigzags back and forth along the sliding surface [14]. In the real world, chattering can cause severe damage to mechanical systems. For example, if a doubly-fed induction generator experiences chattering, it can cause the coils in the generator to overheat [18]. Another example is mechanical flaps on aircraft wings cannot move up and down with a high frequency without breaking into pieces.

One possible solution to smooth out chattering is to replace the discontinuous function sgn(σ(*t*)) with a more practical implementation. This can be realized using the approximation,

$$\operatorname{sgn}(\sigma(t)) \cong \frac{\sigma(t)\left(1+\alpha\,|\,\sigma(t)\,|\right)}{1+|\,\sigma(t)\,|\left(1+\alpha\,|\,\sigma(t)\,|\right)}, \quad \alpha \in \mathbb{R}^{+} \qquad (75)$$

where α is a design parameter which can be selected to control (limit) the hard switching that is causing the extreme chattering.

Using this implementation for sgn(σ(*t*)) results in a smoother control function, however it cannot provide finite-time convergence of the sliding variable to zero in the presence of external disturbances. This means that the attenuation of chattering does cause a small loss in robustness and accuracy, however this seems a reasonable trade off in order to avoid complete destruction of a mechanical system. In conclusion, the control law $i_{qr}(t)$ now has three design parameters, s, β, and α. Figs. 7 and 8 show the simulation results of the control signal as well as the

achieved rotational speed when using the modified sign function with α = 50. Fig. 9 shows the instantaneous generated power after applying our sliding mode control signal. The average generated power is 6.24 kW, which is slightly lower than that obtained when the ideal optimal control [12] is applied (6.46 kW). This is may be due to the fact that the design parameters have not yet been tuned to maximize generator efficiency.

Although the power generated by the OWC WEC with the generator mounted on the turbine using the proposed sliding mode controller is slightly less than that generated by the OWC WEC using the ideal controller, the average efficiency of the former is higher than that of the latter, namely, 91.97% versus 84.65%.

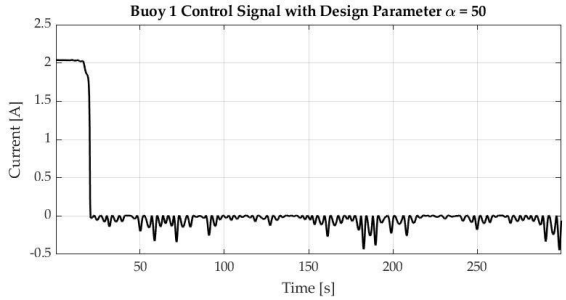

Fig. 7. q-axis rotor control current.

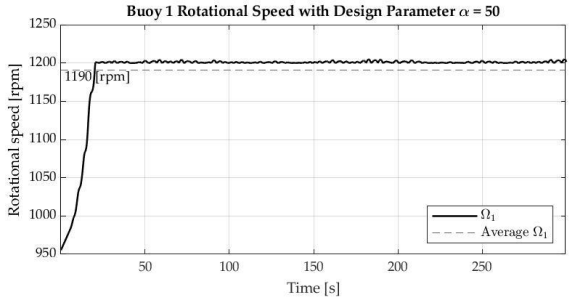

Fig. 8. Buoy 1 rotational speed.

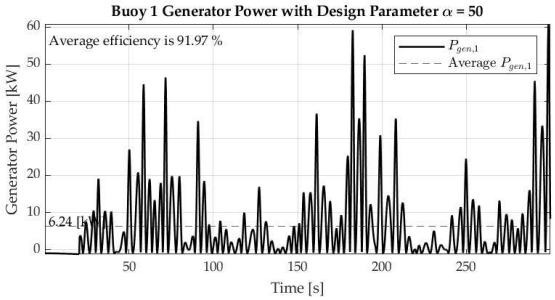

Fig. 9. Buoy 1 instantaneous generated power.

Figure 10 depicts the generator output power of buoy 1 for varying wave incidence angles over the course of 5 minutes using the tuned SMC. We can see that the generated power of buoy 1 decreases only slightly when it is in the shadow of buoy 3.

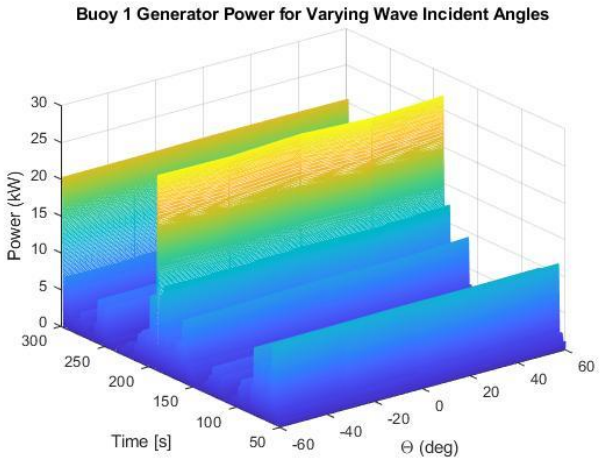

Fig. 10. Buoy 1 tuned SMC generator power at varying wave incidence angles.

VI. CONCLUSION

The SMC controller was successfully validated and compared to an ideal theoretical controller. The results showed that our controller increased the output power of the generator of each WEC by about 100W. The design parameters of each controller were further tuned for different wave incidence angles, in order to optimize the power output of each WEC for every wave excitation.

APPENDIX

Model Parameters

ρ_w = 1025 kg/m^3
ρ_{at} = 1.2041 kg/m^3
γ = 1.4
d = .5 m
H_s = 2 m
T_s = 10 s
S_b = 19.635 m^2
S_p = 6.2458 m^2
K = 80000 N/m
β = 60 degrees

REFERENCES

[1] A. von Jouanne and T. K. A. Brekken, "Ocean and geothermal energy systems," *Proceedings of the IEEE*, pp. 1–19, 2017.

[2] L. Rusu and F. Onea, "The performance of some state-of-the-art wave energy converters in locations with the worldwide highest wave power," *Renewable and Sustainable Energy Reviews*, vol. 75, pp. 1348–1362, Aug 2017.

[3] J. Hals, J. Falnes, and T. Moan, "Constrained optimal control of a heaving buoy wave-energy converter," *J. Offshore Mech. Arct. Eng.*, vol. 133, pp. 1–15, Feb. 2011.

[4] E. Abraham and E. C. Kerrigan, "Optimal active control and optimization of a wave energy converter," *IEEE Trans. Sustain. Energy*, vol. 4, no. 2, pp. 324–332, Apr. 2013.

[5] M. Richter, M. E. Magaña, O. Sawodny, and T. K. A. Brekken, "Power optimization of a point absorber wave energy converter by means of linear model predictive control," *IET Renew. Power Generation*, vol.8, no.2, pp.203– 215, Mar. 2014.

[6] M. Richter, M. E. Magaña, O. Sawodny ,and T. K. A. Brekken, "Nonlinear model predictive control of a point absorber wave

energy converter," *IEEE Trans. Sustain. Energy*, vol. 4, no. 1, pp. 118–126, Jan. 2013.

[7] M. Foley and T. Whittaker, "The effects of sub-optimal control and spectral wave climate on the performance of wave energy converter arrays," Applied Ocean Research, vol. 31, no. 4, pp. 260-266, Oct. 2009.

[8] T. Ahmed and A. F. Zobaa, "Offshore power conditioning system connecting arrays of wave energy converters to the electric power grid," Proc. 8th *Int. Conf. Adv. Power Syst. Control Oper. Manage*. (APSCOM'09), 2009, pp. 1–6.

[9] E. Ransley and D. Greaves, "Investigating interaction effects in an array of multi-mode wave energy converters," *Proc. 27th Int. Workshop Water Waves Float. Bodies*, Copenhagen, Denmark, Apr. 2012.

[10] R. P. F. Gomes, J. C. C. Henriques, L. M. C. Gato, and A. F. O. Falçao,"Hydrodynamic optimization of an axisymmetric floating oscillating water column for wave energy conversion," *Renewable Energy*, vol. 44, pp. 328–339, 2012.

[11] J. Henriques, R. Gomes, L. Gato, A. Falc˜ao, E. Robles, and S. Ceballos, "Testing and control of a power take-off system for an oscillating-water-column wave energy converter," Renewable Energy, vol. 85, pp. 714–724, Jan 2016.

[12] D. T. Gaebele, "Modelling of an array of floating oscillating water column wave energy converters with full hydrodynamic coupling and nonlinear power take off dynamics," MS thesis, University of Stuttgart, Stuttgart, Germany, 2018.

[13] W. Qiao, W. Zhou, J. M. Aller, and R. G. Harley, "Wind speed estimation based sensorless output maximization control for a wind turbine driving a DFIG," *IEEE Trans. on Power Electronics*, vol. 23, no. 3, pp. 1156-1169, 2208.

[14] Y. B. Shtessel, C. Edwards, L. Fridman, and A. Levant, Sliding Mode Control and Observation. 2014.

[15] D. R. Brown, "Sliding mode control of oscillating water column wave energy converters," MSEE thesis, School of EECS, Oregon State University, Corvallis, OR, 2018.

[16] A. J. Garrido, I. Garrido, M. Amundarain, M. Alberdi, and M. De la Sen, "Sliding mode control of wave power generation plants," *IEEE Transactions on Industry Applications*, vol. 48, pp. 2372–2381, November 2012.

[17] Z. Mi, L. Liu, H. Yuan, P. Du, and Y. Wan, "A novel control strategy of DFIG based on the optimization of transfer trajectory at operation points in the islanded power system," *Mathematical Problems in Engineering*, vol. 2016, pp. 1–10, March 2016.

[18] E. Bounadja, A. Djahbar, and M. Matallah, "Direct torque control of saturated doubly-fed induction generator using high order sliding mode controllers," *IJACSA) International Journal of Advanced Computer Science and Applications*, vol. 7, no. 7, 2016.